



Effect of Shot Peening on Residual Stress Distribution and Microstructure Evolution of Artificially Defected 50CrV4 Steel

Simge Gencalp Irizalp, Nursen Saklakoglu, Fatih Baris, and Selda Kayral

(Submitted April 7, 2020; in revised form September 25, 2020; accepted October 4, 2020; published online November 2, 2020)

The aim of this paper is to clarify the effects of shot peening on fatigue life and strain hardening behavior of spring steel samples containing artificial surface defect. Artificial defect acting as pre-cracks is introduced and the effects of this defect on the material surface and the distribution of residual stress away from the defect are investigated before and after shot peening. Shot peening has provided the following modifications on the surface: (1) homogenous compressive residual stress, (2) high dislocation density, (3) superficial strain hardening, (4) retained austenite reduction. In this paper, shot peening is applied to 50CrV4 steel and its effect on surface roughness, microhardness, surface residual stress, crystallite size and dislocation density calculation is determined and SEM observations are used to reveal the properties severely strain-hardened layer. It can be shown that the shot peening can modify the crystallite size, however, the main effect is achieved by increasing the dislocation density and inducing the highly compressive residual stress. The effect of the surface modification to the 3-point bending fatigue life are analyzed.

Keywords fatigue test, residual stress, shot peening, surface defect, surface strain-hardening

1. Introduction

Fatigue is the most common mechanism of damage in mechanical structures that causes sudden breakdowns. For this reason, a lot of research has been made to examine the fatigue behavior of the materials. Many processes have been applied to increase the fatigue performance of the components. Shot peening (SP) is a mechanical surface treatment method that is widely used especially in the automotive and aerospace industries. SP is a process that improves the fatigue durability of components by modifying the surface (Ref 1). In this technique, the material surface is bombarded with small, hard, and high-speed spheres called shots, so localized inhomogeneous severe plastic deformation is induced at the specimen's surface (Ref 2). The adjacent deeper material that borders around the localized plastic deformation produces surface compressive residual stress field (Ref 3, 4). Compressive residual stresses improve the fatigue strength by increasing the resistance to surface crack initiation and also propagation (Ref 5-7). Soady (Ref 8) presented the review of the effects of the SP process on surface roughness, strain hardening, and compressive residual stresses. It is stated that the benefits of compression type residual stresses and strain hardening resulting from SP are predominant over any detrimental effect on fatigue life,

usually caused by surface roughness. In addition, ultra-fine grained structures and sub-grains have attracted considerable scientific interest in surface damages. Trško et al. (Ref 9) showed a significant reduction in crystallite size by severe SP, while no significant increase in the field of compressive residual stress has been achieved. It is well known that the fatigue properties of the materials are very sensitive to grain size (Ref 10, 11).

Low alloy high strength steels have good toughness and formability. For these steels, it has been reported that the fatigue crack usually starts from a large non-metallic inclusion in many studies (Ref 12, 13). Inclusion can be the origin of internal fractures. The stress concentration between inclusion and matrix is the source of fatigue cracking. Another factor that encourages fatigue crack initiations, as well as internal defects, is surface defects. The presence of notches or the presence of the defects on the surface of the structural components also causes stress concentration. On smooth surfaces, the crack starts from the defects on the surface and in this case the fatigue strength of the surface layer of the material changes. This phenomenon, called the notch effect, is associated with the size and shape of the surface defects (Ref 14, 15). Under cyclic loads, these stress concentrations cause crack initiation and can lead to catastrophic damage with crack progression (Ref 16). Benedetti et al. (Ref 17) determined the residual stresses by applying SP to Al-7075-T651 alloy which contained V-notch. Jimenez et al. (Ref 18) performed laser peening on 2205 duplex stainless steel samples and found that the fatigue strength of notched samples improved by 402%. Spring steels for automotive applications are usually shot-peened before use. Non-metallic inclusions, shot peening, decarburized layer and very small pits that develop on the surface through corrosion affect the fatigue strength and many other performance of the real product. SP brings compressive residual stresses, deformation hardening and changes in surface properties. Particularly the

Simge Gencalp Irizalp, Nursen Saklakoglu, Fatih Baris, and Selda Kayral, Department of Mechanical Engineering, Celal Bayar University, 45140 Muradiye, Manisa, Turkey. Contact e-mails: simge.gencalp@cbu.edu.tr, nursen.saklakoglu@cbu.edu.tr, fthbrs@yahoo.com, and selda.kayral@cbu.edu.tr.

effect of the inevitable decarburization layer due to the heat treatment in spring steels and the relationship between the factors can be complicated. Wang et al. (Ref 19) showed that SP treatment can not only introduce large compressive residual stress on the surface of the treated sample but also modify the retained austenite content, and microstructure near the surface region. Decarburization is not origin stress concentration unlike flaws, scratches, defects and non-metallic inclusions, but it decreases the surface hardness and deteriorates the fatigue strength on the average (Ref 20). In a recent study, Lv et al. (Ref 21) also showed that through SP treatment, the fraction of retained austenite of 20CrMnTi steel gear was reduced in the surface layer and they pointed out that the yield strength values of the materials were related to the residual stress produced after modification. The studies concerned with the improvement of surface defects (Ref 14, 22). Although the SP process is a conventional method, it is highly attractive for the materials which have defects that create stress concentration and reduce surface strength. There are few studies that investigated the defect on the SPed surfaces. However, there are no studies about the application SP process on the defected surfaces. The researches on RS distribution of the SP processing on the defected surface is valuable in terms of fatigue life. This is what makes this study important. In this study, the effects of artificially produced surface defect on fatigue threshold were investigated on not peened (as-received) and shot-peened spring steel specimens. The area affected by artificial surface defects and the pre-existing residual stress field have been investigated together because the local material properties of the material affect the fatigue performance. In this study, not only the residual stresses but also how the grain-refined layer just below the surface changes with the artificial surface defect have been revealed.

2. Material and Method

Spring steel SUP10 as per JIS G 4801 or DIN 50CrV4 in Germany with the following chemical compositions mass (%): C 0.47-0.55, Mn 0.70-1.1, Cr 0.90-1.20, V 0.10-0.20, Si 0.4 (max.), P 0.035(max.), S 0.030(max.) and balance Fe was considered in this study. The yield strength, tensile strength, ductility and hardness of quench and tempered 50CrV4 steels are 1262, 1342 MPa, 21.2% and 460 HV, respectively. After the machining process, the samples were subsequently oil-quenched at 900 °C. After this process, the hardness of the samples has reached approximately 58 HRC. Degreasing was carried out before tempering. The as-quenched samples were tempered at 400 °C for 180 min and after this process, the hardness of the samples reduced approximately 45 HRC. After heat treatment, an artificial defect was created with a cutting tool in the middle of the specimens; the defect was rounded tip 150° V notch with a nose radius of 0.895 mm of groove with 0.4 mm depth size.

Experimental three-point bending fatigue tests were performed in specimens with artificial surface defect and non-defect. Stress amplitudes that have been studied correspond to 74-62-50% of the material's 0.2% offset yield strength. Figure 1 (a) shows the dimensions of the fatigue test specimens and the artificial defect. Figure 1(b) shows the SEM image of the defect on the material surface. The sheet-shaped 50CrV4 material has been cut by laser beam. The artificial defect on the specimen is

also seen in Fig. 1. This defect was executed via drill at specimen's center after heat treatment. The hole diameter (d) changes with height (h). In this study, h was set as 0.4 mm and d was measured as 3 mm. The three-point bending tests were performed in Sincotek Power Singly 20 Mot machine with a frequency 45 Hz at room temperature. The specimens were fatigued at a constant maximum stress until failure or if the sample did not fail, the test run out at ± 1 Hz threshold.

The spring steel specimens were subjected to SP process after heat treatment. Two different situations have been created for each geometry with artificial defect (AD) and non-defect (ND). Peening was carried out using S230 steel shot with 50-55 HRC hardness. The size of the steel shots was 0.6 ± 0.1 mm. Impingement angle was set to be 40° and the distance from the nozzle to the workpiece was constant at 500 mm. The specimens were peened for 30 s in both surface during peening operation. Surface images were captured by stereo microscopy after SP. Microstructure observations were performed by a Zeiss EVO50 SEM. Specimens for SEM examinations were etched by 3% nital. After SP, the surface properties of the samples were determined by roughness (Mitutoyo Surf Test SJ-301), microhardness-depth profile and x-ray diffraction (XRD) analysis. The surface roughness test was performed on a different location to determine R_a and R_z of the samples. Microhardness tests were also performed with a 50gf load on not-peened (NP) and shot peened (SP) specimens by a FM-700 Future-Tech Corp device. Differences in crystallite size cannot be observed by optical methods. Therefore, in this study, the NP and SP samples were also characterized by XRD to analyze the crystallite size and dislocation density. This approach is based on using full width at half maximum (FWHM) on intensity peaks from XRD data (Ref 23). The FWHM was measured from the surface on (211) diffraction lattice plane. The residual stresses at the surface depending on the distance away from the artificial defect were measured by using Stresstech Xstress equipped with Cr-K α radiation (wavelength 2.290 Å) with the $\sin^2\psi$ method. Young's modulus and Poisson's ratio which was set to 210GPa and 0.30, respectively, in the stress calculation. Bragg angle was 156.11°. ψ is the angle between normal of the surface and normal of the diffraction plane. ψ angle can be set between $\pm 90^\circ$, however, it is not used over 45 degrees due to the loss of intensity (Ref 24, 25). The sample was rotated at angles of $\psi = \pm 45^\circ, \pm 40^\circ, \pm 35^\circ, \pm 30^\circ, \pm 24^\circ, \pm 17^\circ, 0^\circ$ during the residual stress analysis. The stress measurements were performed at different orientations of $\Phi = 0^\circ, 45^\circ, 90^\circ$ at the same location. Panalytical Empyrean XRD using Cu-K α radiation (voltage: 45 kV, wavelength: 1.542 Å, scanning angle 20°-100°) device was also used for the XRD pattern and phase analysis.

3. Results and Discussion

3.1 Surface Roughness

Figure 1(c) and (d) shows the SEM micrographs of NP and SP specimen's surfaces. The NP surface demonstrates the polished sample after heat treatment. However, the sample surface is very rough, even rolling marks are outstanding. Because polishing is done only for descaling after heat treatment. Surfaces of SP samples have shots marks. These marks seem to have concave-convex texture. These concave-

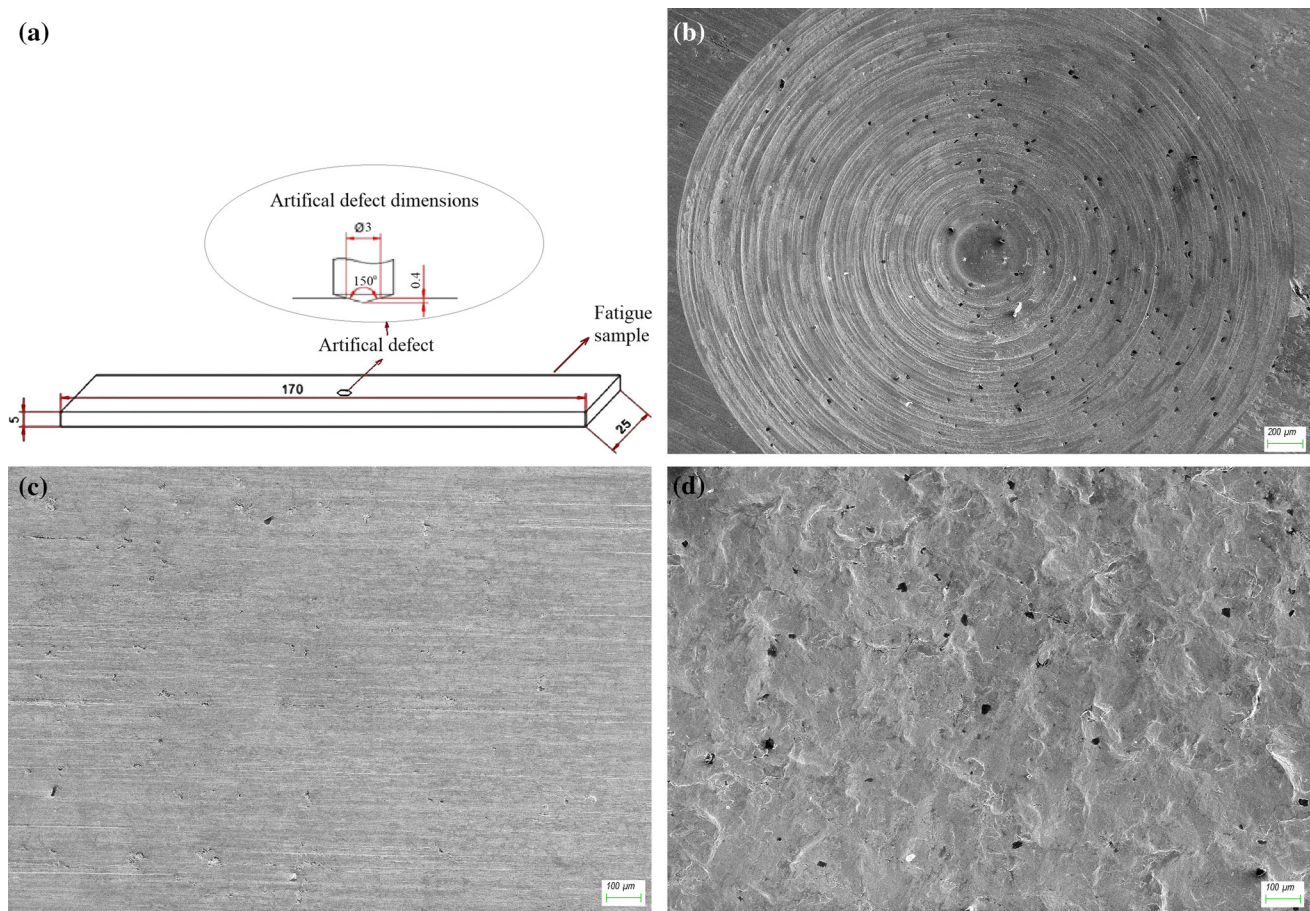


Fig. 1 Shape and dimensions (mm) of a 3-point fatigue test specimen and artificial defect (a), SEM image of the defect (b), SEM images of the material surface (c) NP (d) SP

convex textures develop as a result of the exposure of the surface to the shot flow during the SP and therefore the interaction of the shot impacts. Surface roughness has been measured three times on three samples. The frequently measured and indicated parameters of the surface roughness profile are determined with the values, R_a and R_z (Ref 26-28). The surface roughness values and standard deviation are presented in Table 1. Accordingly, the average surface roughness has increased considerably after SP and has increased to 2.5 μm . Maximum roughness was 13 μm after SP. It demonstrates that SP induces micro-scale indentations on the rolled 50CrV4 spring steel.

3.2 Strain Hardening

The microstructural examination of NP and SP specimens is presented in Fig. 2. When the cross sections were examined for the general microstructural evaluation of the base material, high tempered martensite and retained austenite phases with few carbides were formed due to heat treatment. Figure 2(b) shows the microstructure of the surface modified after SP. It is noteworthy that the grain structure is relatively thinner, so the general refinement of martensite is evident through the sub-surface depth. Figure 3(a) shows a close-to-surface portion of the sample and Fig. 3(b) shows a mid-to-surface portion after SP. When looking carefully at Fig. 3, it is clearly seen that the sub-surface martensite laths are thinner in SP treated material

compared to the middle part of the sample. The change in the amount of retained austenite can be easily distinguished. Mostly the amount of retained austenite in SP microstructures is reduced at a shallow depth on the surface. Phase analysis was carried out via XRD to investigate the change of these phases on the surface. The XRD patterns of the SP and NP specimens are presented in Fig. 4. From Fig. 4, it can be observed that all intensity diffraction peaks were indexed as α' -martensite. These patterns have peak positions similar to the α -Fe phase. Moreover, the patterns included the peak of γ -Fe phase and this phase indicates the retained austenite. In SP specimens, there was no γ -Fe peaks in XRD pattern. It means that the retained austenite reduced by phase transformation. These findings are very well-related to SEM microstructures.

The SP modifies the structure into an ultra-fine crystallized structure in a very shallow layer near the surface. Hence, there is a coarse-grained interior under the nanostructured surface layer after the SP treatment. This nano-structure cannot be certainly observed with SEM. Therefore, the crystallite size of the surface can be analyzed by x-ray diffractometer. This approach is based on obtaining full width at half maximum (FWHM) on the severe XRD peak and calculating the crystallite size, micro-strain and dislocation density. The crystalline size distribution of the material and instrumental errors affect the diffraction peak width and it refers to the micro-strain indirectly (Ref 29). It is possible to calculate the crystallite size and micro-strain by Scherrer equations (Ref 30).

The equations are $\beta = \frac{K\lambda}{L \cos \theta}$ and $\beta = C\epsilon \frac{\sin \theta}{\cos \theta}$ where the peak width β , λ is the wavelength of x-ray and K is the Scherrer constant, which is assumed to be approximately 0.94. A crystallite size is the main size of consistently diffracted domains in crystals. Therefore, grains may contain several domains separated by a small angle misorientation and these can be considered as the subgrain boundaries (Ref 31).

FWHM is the width of diffraction peak, in radians, at a height halfway between background and the maximum peak. β consists of the contribution of the crystallite size L and micro-strain ϵ . The C value is constant and typically 4 (Ref 30). In addition, changing dislocation density with SP effect is determined indirectly by x-ray line analysis. The dislocation density is defined as the length of the dislocation lines per unit area of the crystal (Ref 23, 30-33). Severe plastic deformation effect during SP increases the dislocation density in the near surface region. The dislocation line density δ can be calculated from the crystallite size L by $\delta = \frac{1}{L^2}$ equation (Ref 23, 31-33).

By means of these equations, the crystallite size L , lattice micro-strain ϵ and dislocation density δ were determined with reference to the peaks of the (211) lattice plane which is the peak at which residual stress measurements were performed. The width of diffraction peak increases as a result of an increase in micro-strain induced by plastic deformation (Ref 23, 32, 33). We found that the increase in lattice micro-strain is 23.23% when compared to that of the not peened samples. Severe plastic deformation that produced by SP in the restricted area distributes the orientations of the crystallites, increases the dislocation density, and causes the rearrangement of the subgrain boundaries (Ref 34). It can be seen from Table 2, the dislocation density noticeably increased by 52% due to SP, while the crystallite size reduced 18%. The change in the size of the crystallites is not as striking as the change in the dislocation density. The higher dislocation density arose from multiple SP impacts. As plastic deformation increases, the amount of strain increases resulting in subdivision of original coarse grains into sub-grains with dislocation tangles and dense dislocation walls. The total energy due to repeated shots is minimized by the dislocation annihilation by the formation of multiple shear bands, which further divide sub-grains into ultra-fine grains with high angle grain boundaries (Ref 35). When this energy is not spent on the new nanostructured layer formation, dislocation density can be higher (Ref 36). Therefore, it is constructive that the grains are not refined in large proportions in order to obtain large amounts of compressive residual stresses. The dislocation multiplication occurred with the increase of plastic deformation and the compressive residual stress is induced by the oppression among grains (Ref 36). These results show that the induced energy is active in producing residual stresses by pressing on increasing the dislocation intensity.

Figure 5 shows the microhardness distribution of the NP and SP samples in the depth direction. The hardness did not change remarkably from the surface to the material's center. The presence of a decarburization layer on the surface is clear, and with the effect of SP, there is some increase in the hardness of

this layer. These measurement results allow us to comprehend the hardening increase just below the surface approximately 150 μm caused by SP. Decarburization is often accompanied with the undesirable metallurgical condition of retained austenite. As a matter of fact, the presence of retained austenite appeared in NP samples was exhibited by XRD phase analysis. However, it was found that retained austenite amount decreased after shots impacts. Thanks to peening impact, strain-induced martensite transformation occurred. As a result, part of the retained austenite is transformed into strain-induced martensite, the crystallite size is reduced and the dislocation density is increased in the surface layer. It is well known that SP is an effective method to eliminate retained austenite that develops on the surface (Ref 19, 21). Sometimes the prior austenite grains boundary could also be a crack origin for high-carbon chromium steel under low tempering temperature (Ref 37). Consequently, decreasing the amount of residual austenite is also useful in this regard.

3.3 Surface Compressive Residual Stress and the Effect of Artificial Defect

After the crystallite size, micro-strain and dislocation density were explained, the residual stresses which were an important output after the SP process, were evaluated. Soady (Ref 8) discussed about the relationship between maximum compressive residual stress and yield stress of the material. Residual stress magnitude is clearly associated with the yield stress of the material. As the yield stress of the material increases, the final residual stress value will increase. In this study, it is inevitable that the yield stress value of the decarburization layer just below the surface is lower than the main material. The surface values of FWHM is increased with SP (as shown in Fig. 6). The increase in the FWHM value is not as radical as the residual stress, only reflects a decrease in the not aligned dislocations at the subgrain boundaries. FWHM is also related to microstrains and is assumed as an index of hardening of the material (Ref 38). The variation in FWHM depending on the distance from artificial defect in 50CrV4 before and after SP was demonstrated in Fig. 6. The artificial defect resulted in no significant variation in the FWHM.

In this study, residual stress values before and after SP as the distance from the artificial surface defects are given in Table 3. SP influenced the residual stresses. While the variations in the crystallite sizes are less before and after SP, the residual stress has risen to -500 MPa levels, considering the residual stress values in the same region. These values are quite high for a spring steel with a decarburized zone. When the dislocation structure turns into the formation of new nanograin boundaries, the energy of the structure reduces and residual stress values are at lower levels (Ref 31). However, when this energy is not spent on the new nanostructured layer formation, residual stresses may be in higher levels. Li et al. (Ref 36) concluded that the maximum compressive residual stress is located in incompletely refined grains. The dislocation annihilation, as a result of the grain refinement, leads to the reduction of

Table 1 Roughness values and standard deviation

Treatment	R_a , μm	R_z , μm
Not peened	0.219 ± 0.02	1.687 ± 0.23
Shot peened	2.50 ± 0.17	13.179 ± 0

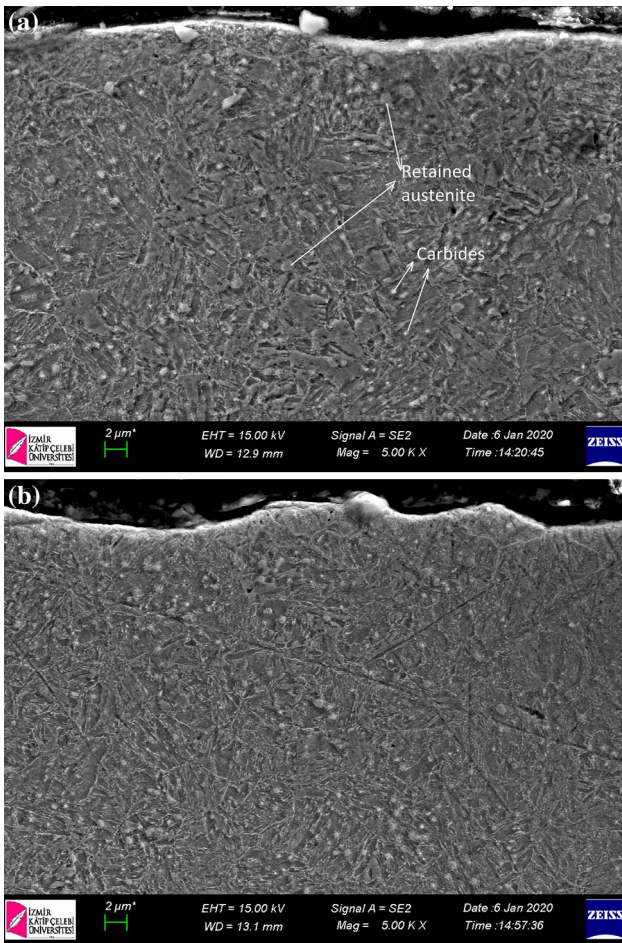


Fig. 2 Cross sectional SEM microstructure of (a) NP, (b) SP

compressive residual stresses. The change in the crystallite size does not make a significant difference (about 18% reduction occurred, as given in Table 2) and the high level of residual stress in the decarburized layer (about -500 MPa) indicates that this energy is spent on residual stress formation.

In NP samples, as it moves away from artificial defect, the maximum compressive residual stress on both 0° , 45° , 90° shows an anisotropic stress generation resulting from the manufacturing process and heat treatment of the samples. Residual stress values at a distance close to the artificial surface defect ($250 \mu\text{m}$) vary as high as 35 times depending on the stress direction. At a distance of $3000 \mu\text{m}$, while the residual stress value was in the direction of 90° was -196 MPa, it was about 26 MPa in the direction of 0° . These results show that there is a significant anisotropy on the material surface after manufacturing and heat treatment processes the spring steel. Initial surface residual stresses are highly directional. It is clear that these residual stresses are not only dependent from the rolling direction. The directional variation of σ_x and σ_y stresses varied due to the tempering heat treatment and rolling process. Lesser anisotropy is clearly evident after SP treatment. The formation of more homogeneous strain areas during SP (the fact that many balls act in the same place with the plastics deforming region and the elastic deforming region around it create a homogeneous stress area) triggered more homogeneous residual stress. Gencalp Irizalp et al. (Ref 39) induced laser

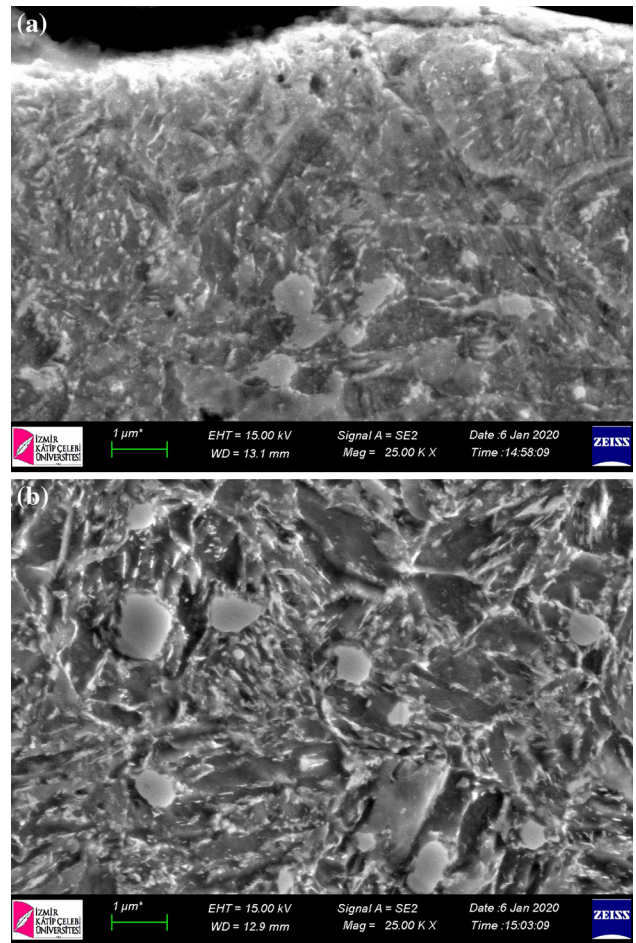


Fig. 3 SEM microstructures in the sub-surface region (a) and the center region (b) of the SP specimen

peening to the 6061-T6 alloy and reported that an anisotropic stress generation led to anisotropic plastic deformation after peening. This situation can be associated with SP as follows: The SP process executes randomly peening the surface of the shots allows a homogeneous stress field to occur. The other remarkable result was that the residual stresses were highest on the $1500 \mu\text{m}$ away from defects for all directions tending to be tensile type especially in not peened samples. After that, the residual stresses were stabilized. The defect is effective in a $1500 \mu\text{m}$ diameter. After SP, that effect decreased significantly (Fig. 7).

3.4 Fatigue Performance

3-point bending fatigue tests have been performed at room temperature on the NP and SP samples with defect and no-defect. Results of fatigue tests, stress versus number of cycles to failure or run-out are given in Table 4. The results obtained from fatigue tests clearly indicated that fatigue life of the samples was improved by SP. SP has improved the fatigue strength in case of artificial defect. Fatigue life improvement is 9 times in non-defect materials, while it is 4.5 times in materials with artificial defect. These results are attributed to the high-level compressive residual stress and strain-hardened surface layer. Fatigue life was substantially sensitive to near-surface residual stress (Ref 40). As expected, introducing an artificial

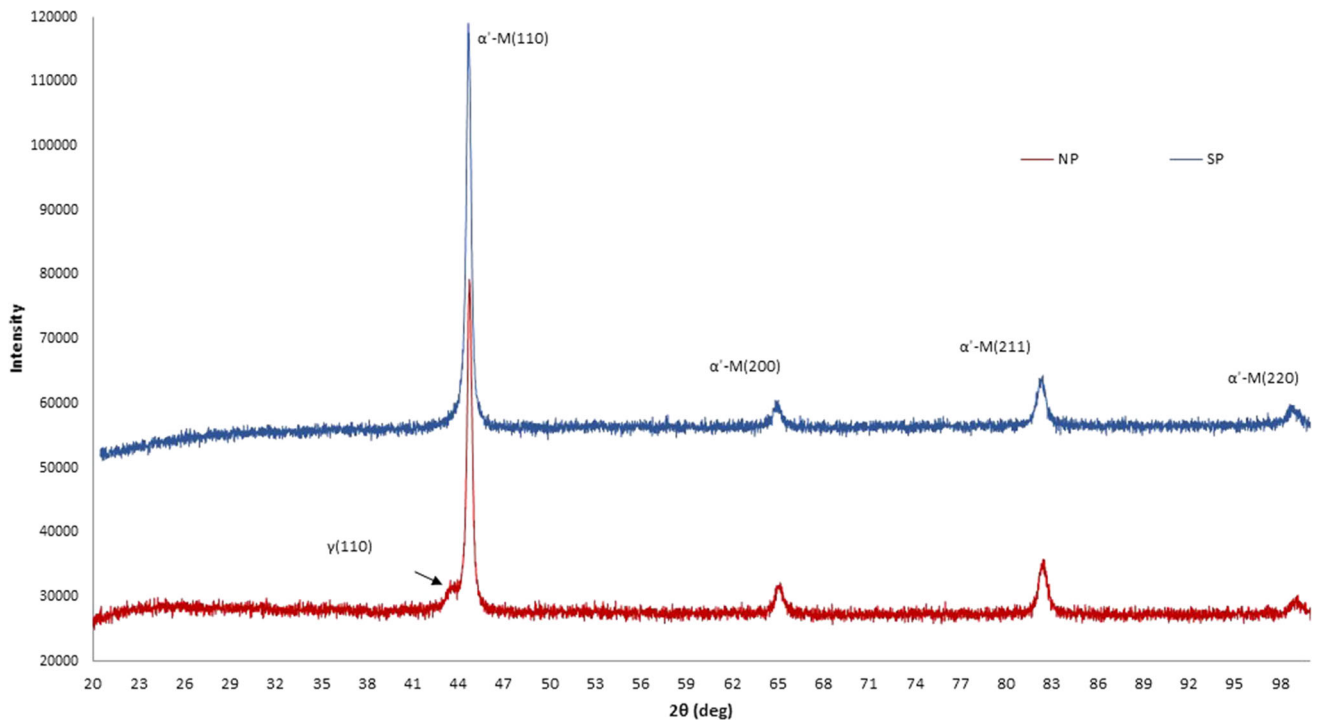


Fig. 4 X-ray diffraction (XRD) patterns of specimens

Table 2 The value of FWHM, crystallite size L and dislocation density δ on non-defect surface

Treatment	FWHM, °	Crystallite size L , nm	Micro-strain ϵ , %	Dislocation density δ , 10^{14} lines/m ²
Not peened	2.616	22.807	0.409	19.223
Shot peened	3.216	18.539	0.504	29.096

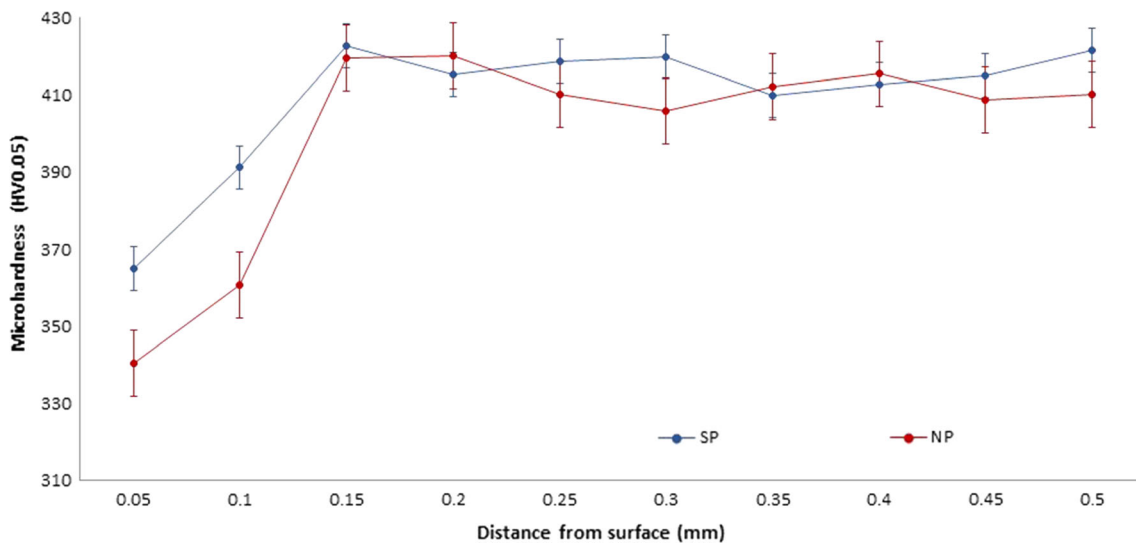


Fig. 5 Comparison between SP and NP microhardness in thickness direction

defect on material surface worsens fatigue performance in terms of service life. The fatigue performance is affected by fatigue crack nucleation. Grain refining and high-level compressive residual stresses developed after SP clearly postpone fatigue crack nucleation (Ref 41-43). In fine-grained and especially

nano-crystalline materials, both internal and surface defects have been reported as nucleation sites for fatigue cracks (Ref 15). After fatigue testing, it is seen that fractures have started from artificial surface defects. The refined grain structure and nano-crystalline structure developed by the SP process closed

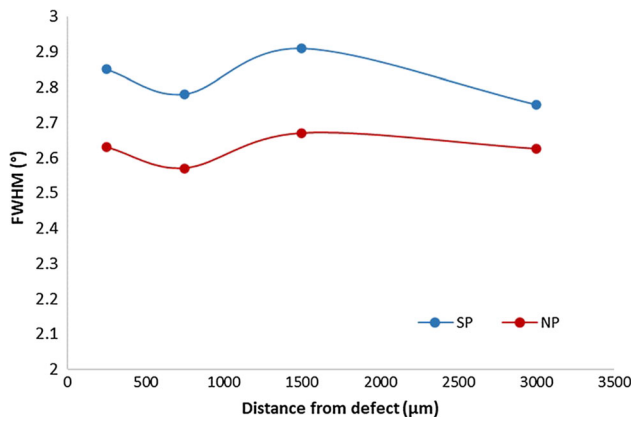


Fig. 6 FWHM profile, expressed in degree (°) in-distance from defect trend, before and after SP

the cracks and discontinuities remaining on the surface of the non-artificial defect specimen and also delayed the crack initiation in the near surface layer. The presence of compressive residual stresses also delays crack propagation (Ref 44). An artificial surface defect creates a relatively high stress concentration and crack begin from the defect. Looking at the literature, some studies have reported that when the notch geometry is small, the high stress gradient formed at the bottom of the notch causes crack closure by residual stresses after SP, and thus the fatigue strength of the SP treated materials increases (Ref 15, 45). Takahashi et al. (Ref 45) found that when the specimens having a notch less than 0.2 mm, the fatigue crack after SP started from outside the notch. And it has also been determined that the fatigue limit is equal to the unnotched samples. There is considerable fatigue resistance thanks to SP treatment. As a result, the SP process both increased the fatigue limit and reduced the failure from surface

Table 3 Surface residual stress values for specimens

Defect condition	Distance from defect, μm		Stress σ_{res} , MPa	
			Not peened	Shot peened
AD	250	0°	-4.3 ± 14.4	-411.9 ± 8.9
		45°	-62.2 ± 9.0	-443.3 ± 7.9
		90°	-149.7 ± 6.4	-439.1 ± 8.4
AD	750	0°	70.3 ± 9.1	-431 ± 6.0
		45°	-35.3 ± 12.9	-443.4 ± 5.5
		90°	-123.6 ± 5.0	-447.5 ± 10.6
AD	1500	0°	114.9 ± 14.7	-423.17 ± 9.5
		45°	-15.7 ± 9.0	-414.5 ± 11.3
		90°	-84.8 ± 6.4	-414.9 ± 7.9
AD	3000	0°	25.7 ± 8.2	-465.9 ± 6.4
		45°	-95.2 ± 11.4	-468 ± 5.4
		90°	-196.1 ± 9.5	-458.6 ± 8.2
ND	...	0°	-20.4 ± 8.7	-470.4 ± 7.6
		45°	117.7 ± 10.1	-501.1 ± 10.6
		90°	-198.3 ± 17	-487.4 ± 8.5

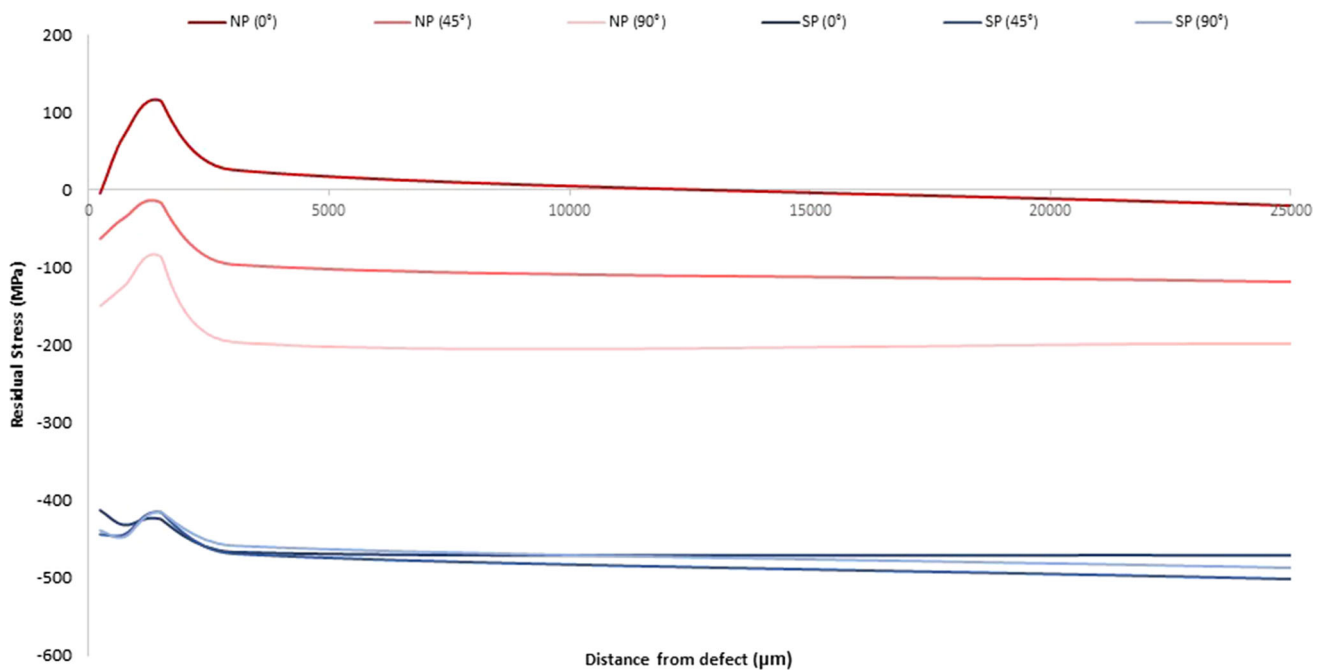


Fig. 7 Residual stress distribution away from the defect

Table 4 Results of fatigue tests

Stress amplitude, MPa	Fatigue cycle			
	ND	AD	ND+SP	AD+SP
1008	99,757	58.930	321.141	144.056
840	191.560	94.000	683.699	329.087
672	320.600	231.337	2.891.960	1.076.757

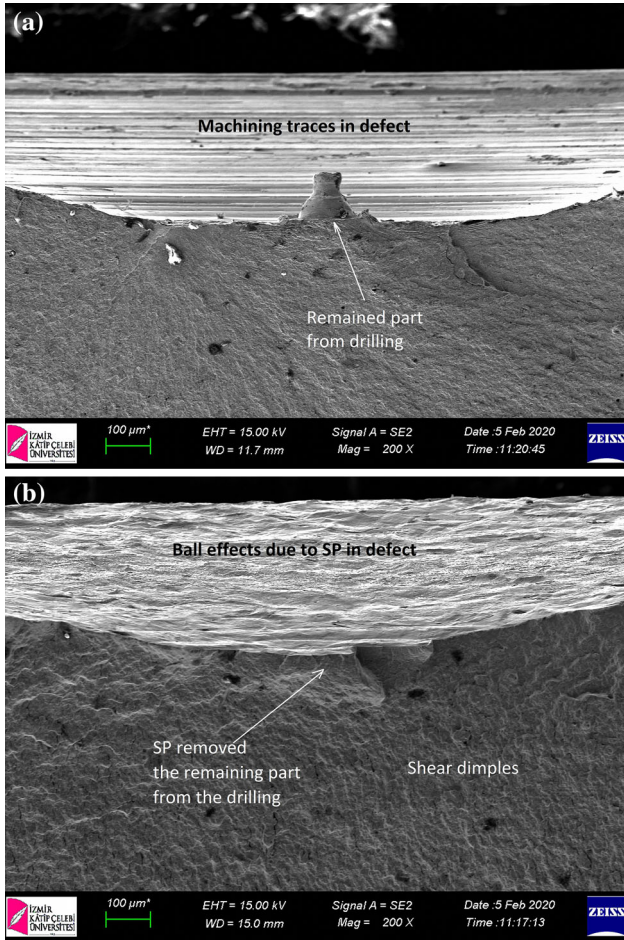


Fig. 8 Fractured surface of (a) artificial defected and not peened specimen; (b) artificial defected and shot peened specimen

flaws in small notches. In this study, the depth of the artificial surface defect in our study is 0.4 mm and surface area of the defect is wide. The damage occurred in artificial surface defects for both NP and SP samples. The reason for this is related to the defect sizes. If the size of the surface defects is adequately small compared to the area affected by the SP shots [for example FIB-milled notched (Ref 46)], the defects have not notably changed the fatigue strength of the SP specimens. However, if the surface defect is in an area where SP impacts can affect, then with SP treatment, the product can be used with a better service life than even the non-defect material. We found that the defect was effected by ball hits during SP treatment and the shear dimples were dominant under the defect on the fractured surface (Fig. 8). Therefore while AD sample showed 231.337 cycle for 672 MPa stress level, it was 1.076.757 cycle after SP

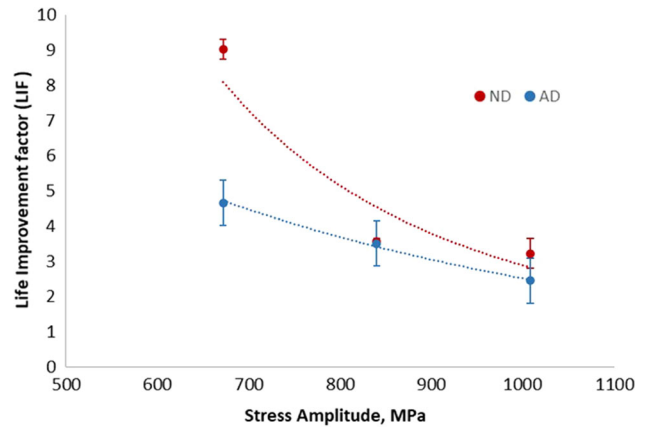


Fig. 9 3-point bending fatigue curves of shot peened and not peened specimens

corresponding to 365% improvement of fatigue life. Considering that the fatigue life of the ND sample is 320.600 cycle, it can be said that the SP treatment completely eliminates the negative effect of the defect on the fatigue life. When an expensive or critical component is notched during manufacturing, assembly, or foreign object damage, it is possible to restore it by producing the compressive residual stress by SP in place of tensile-type stresses caused by damage.

Figure 9 derived from Table 4 shows the life improvement factor LIF ($LIF = N_f/N_{f_0}$ = total life of SP/total life of NP) which was calculated for artificial defect or non-defect the condition. The complete results (LIF) for all loading cases are demonstrated in this curve. The variance of LIF is introduced by means of error bars (vertical lines). It was seen that as the stress amplitude increased, the LIF for ND and AD samples decreased. That shows that the higher stress amplitude resulted lower LIF value for both not-peened and shot peened materials. During cyclic loading (especially compressive loading), however, compressive residual stress relaxation may happen, depending on the applied stress amplitude and the cyclic stress–strain behavior of the material (Ref 47, 48). Torres and Voorwald (Ref 47) observed that the stress relaxation was more significant for the highest applied stress, both at and below the surface. In the case of peening induced compressive residual stress, Bag et al. (Ref 49) reported more than 70% relaxation during the 1st load cycle when a steel sample was subjected to high stress amplitudes. At the chosen stress amplitude of 672 MPa (50% of $\sigma_{y,0.2}$), the magnitudes of LIF were 9 and 4.6 for ND and AD, respectively. Whereas, LIF values were 3.2 and 2.4 for ND and AD for 1008 MPa stress amplitude (74% of $\sigma_{y,0.2}$) which can be referred to higher mechanical relaxation. If the loading stresses reaches the stress required for plastic

deformation because of higher stress level, the relaxation starts (Ref 50). The amount and the rate of relaxation of shot peened surfaces, however, are controlled by the magnitude of the plastic deformation. Therefore, at higher stress amplitudes corresponding to larger plastic strains the residual stresses will be loosening already from the beginning (Ref 51) and cannot make an enough contribution to the fatigue durability (Ref 1), no matter defected or non-defected.

4. Conclusion

The effect of artificial surface defect and the 3-point bending fatigue behavior of NP and SP 50CrV4 spring steel was investigated. Following conclusions can be drawn from this investigation:

1. Microscopic examinations revealed that grain refining was obtained below the surface by SP. XRD line broadening analysis showed the crystallite size reduction and dislocation density increment just below the surface with SP treatment.
2. XRD studies presented the retained austenite reduction at the surface and that is transformed to strain-induced martensite phase after SP.
3. Grain refinement mechanism may be induced by the activity of high dislocation density. In addition, the stored energy with this increase in the dislocation intensity triggers the formation of residual stresses. The greatest compressive residual stresses were developed by the interaction between the dislocation tangles.
4. As it was expected, the residual stress produced as compressive type on the material surface after the SP treatment. The highest residual stress value on the surface is – 501 MPa. This result shows that the stored energy by the plastic deformation effect after SP creates highly effective residual stress even in a decarburized layer.
5. The artificial surface defect certainly reduced the fatigue life. Fatigue damage was also on the artificial surface defect in the samples treated by SP. However, the fatigue life performance in the spring steel can be absolutely increased by using SP. It is possible to restore it by producing the compressive residual stress by SP in place of tensile-type stresses caused by damage.
6. Plastic deformation induced by a SP treatment prominently advances the surface roughness, compressive residual stress and microhardness of the spring steel. These advancements can be referred to the grain refinement and strain hardened layer (crystallite size refinement and dislocation density increment) resulting from SP.
7. The benefit of this process is that it makes the component reusable, especially in components with surface defects, while increasing the fatigue life according to the not-peened and no artificial defect conditions.

Acknowledgments

The authors would like to thank Celal Bayar University (Project Code: 2018-039) for providing financial support and Dönmez Debriyaj company for the preparation of samples.

References

1. K. Dalaei and B. Karlsson, Influence of Shot Peening on Fatigue Durability of Normalized Steel Subjected to Variable Amplitude Loading, *Int. J. Fatigue*, 2012, **38**, p 7583. <https://doi.org/10.1016/J.ijfatigue.2011.11.011>
2. S. Bajda, W. Ratuszek, M. Krzyzanowski, and D. Retrait, Inhomogeneity of Plastic Deformation in Austenitic Stainless Steel After Surface Mechanical Attrition Treatment, *Surf. Coat. Technol.*, 2017, **329**, p 202–211. <https://doi.org/10.1016/J.Surfcoat.2017.09.049>
3. S. Shen and S.N. Atluri, An Analytical Model for Hot-Peening Induced Residual Stresses, *Comput. Mater. Contin.*, 2006, **4**, p 75–85. <https://doi.org/10.3970/Cmc.2006.004.075>
4. K. Zhan, C.H. Jiang, and V. Ji, Uniformity of Residual Stress Distribution on the Surface of S30432 Austenitic Stainless Steel by Different Shot Peening Processes, *Mater. Lett.*, 2013, **99**, p 61–64. <https://doi.org/10.1016/J.Matlet.2012.08.147>
5. E. Delosrios, A. Walley, M. Milan, and G. Hammersley, Fatigue Crack Initiation and Propagation on Shot-Peened Surfaces in A316 Stainless Steel, *Int. J. Fatigue*, 1995, **17**(7), p 493–499. [https://doi.org/10.1016/0142-1123\(95\)00044-T](https://doi.org/10.1016/0142-1123(95)00044-T)
6. A.L.M. Carvalho and H.J.C. Voorwald, Influence of Shot Peening and Hard Chromium Electroplating on the Fatigue Strength of 7050-T7451 Aluminum Alloy, *Int. J. Fatigue*, 2007, **29**(7), p 1282–1291. <https://doi.org/10.1016/J.ijfatigue.2006.10.003>
7. V.M. Radhakrishnan and P.S. Baburamani, Initiation and Propagation of Fatigue Crack in Pre-strained Material, *Int. J. Fract.*, 1976, **12**(3), p 369–380. <https://doi.org/10.1007/Bf00032832>
8. K.A. Soady, Life Assessment Methodologies Incorporating Shot Peening Process Effects: Mechanistic Consideration of Residual Stresses and Strain Hardening Part 1—Effect of Shot Peening on Fatigue Resistance, *Mater. Sci. Technol. Ser.*, 2013, **29**(6), p 637–651. <https://doi.org/10.1179/1743284713y.0000000222>
9. L. Trško, M. Guagliano, P. Lukáč, O. Bokůvka, and F. Nový, Effects of Severe Shot Peening on the Surface State of Aw 7075 Al Alloy, *Kovove Mater.*, 2015, **53**(4), p 239–243. <https://doi.org/10.4149/Km-2015-4-239>
10. P. Zhang, J. Lindemann, and C. Leyens, Influence of Shot Peening on Notched Fatigue Strength of the High-Strength Wrought Magnesium Alloy Az80, *J. Alloys Compd.*, 2010, **479**(1–2), p 380–385. <https://doi.org/10.1016/J.Jallcom.2010.03.079>
11. J.W. Tian, J.C. Villegas, W. Yuan, D. Fielden, L. Shaw, P.K. Liaw, and D.L. Klarstrom, A Study of the Effect of Nanostructured Surface Layers on the Fatigue Behaviors of A C-2000 Superalloy, *Mater. Sci. Eng. A Struct.*, 2007, **468–470**, p 167–170. <https://doi.org/10.1016/J.Msea.2006.10.150>
12. J. Zhang, S. Li, Z. Yang, G. Li, W. Hui, and Y. Weng, Influence of Inclusion Size on Fatigue Behavior of High Strength Steels in the Gigacycle Fatigue Regime, *Int. J. Fatigue*, 2007, **29**(4), p 765–771. <https://doi.org/10.1016/J.ijfatigue.2006.06.004>
13. Q.Y. Wang, J.Y. Berard, S. Rathery, and C. Bathias, Technical Note High-Cycle Fatigue Crack Initiation and Propagation Behaviour of High-Strength Spring Steel Wires, *Fatigue Fract. Eng. Mater.*, 1999, **22**(8), p 673–677. <https://doi.org/10.1046/J.1460-2695.1999.T01-1-00184.X>
14. I. Fernández-Pariente, S. Bagherifard, M. Guagliano, and R. Ghelichi, Fatigue Behavior of Nitrided and Shot Peened Steel with Artificial Small Surface Defects, *Eng. Fract. Mech.*, 2013, **103**, p 2–9. <https://doi.org/10.1016/J.Engfracmech.2012.09.014>
15. S. Bagherifard, I. Fernandez-Pariente, R. Ghelichi, and M. Guagliano, Fatigue Behavior of Notched Steel Specimens with Nanocrystallized Surface Obtained by Severe Shot Peening, *Mater. Des.*, 2013, **45**, p 497–503. <https://doi.org/10.1016/J.Matdes.2012.09.025>
16. Z.Y. Wang, Q.Y. Wang, L. Li, and N. Zhang, Fatigue Behaviour of CFRP Strengthened Open-Hole Steel Plates, *Thin Wall Struct.*, 2017, **115**, p 176–187. <https://doi.org/10.1016/J.Tws.2017.02.015>
17. M. Benedetti, V. Fontanari, B. Winiarski, M. Allahkarami, and J.C. Hanan, Residual Stresses Reconstruction in Shot Peened Specimens Containing Sharp and Blunt Notches by Experimental Measurements and Finite Element Analysis, *Int. J. Fatigue*, 2016, **87**, p 102–111. <https://doi.org/10.1016/J.ijfatigue.2016.01.020>
18. C.A. Vázquez Jiménez, G. Gómez Rosas, C. Rubio González, V. Granados Alejo, and S. Hereñú, Effect of Laser Shock Processing on Fatigue Life of 2205 Duplex Stainless Steel Notched Specimens, *Opt.*

- Laser Technol.*, 2017, **97**, p 308–315. <https://doi.org/10.1016/J.Optlastec.2017.07.020>
19. Z. Wang, C. Jiang, X. Gan, and Y. Chen, Effect of shot peening on the microstructure of laser hardened 17-4ph, *Appl. Surf. Sci.*, 2010, **257**(4), p 1154–1160. <https://doi.org/10.1016/J.Apsusc.2010.07.015>
 20. Y. Yamada and T. Kuwabara, *Materials For Springs*, Springer, Berlin, 2007
 21. Y. Lv, L. Lei, and L. Sun, Effect of Shot Peening on the Fatigue Resistance of Laser Surface Melted 20CrMnTi Steel Gear, *Mater. Sci. Eng. A Struct.*, 2015, **629**, p 8–15. <https://doi.org/10.1016/J.Msea.2015.01.074>
 22. Z.Y. Wang, Q.Y. Wang, and M. Cao, Experimental Study on Fatigue Behaviour of Shot-Peened Open-Hole Steel Plates, *Materials*, 2017, **10**(9), p p996
 23. S.G. Irizalp, N. Saklakoglu, and B.S. Yilbas, Characterization of Microplastic Deformation Produced in 6061-T6 by Using Laser Shock Processing, *Int. J. Adv. Manuf. Technol.*, 2014, **71**(1–4), p 109–115
 24. O. Anderoglu, Residual Stress Measurement Using X-Ray Diffraction. Doctoral Dissertation, Texas A&M University, 2005
 25. A. Küçükylmaz, Experimental Investigation of Residual Stresses Introduced Via Shot Peening and Their Effect on Fatigue Life of Ball Bearings (Master's Thesis), Middle East Technical University, 2010
 26. A. Kubit, M. Bucior, W. Zielecki, and F. Stachowicz, The Impact of Heat Treatment and Shot Peening on the Fatigue Strength of 51CrV4 Steel, *Procedia Struct. Integr.*, 2016, **2**, p 3330–3336
 27. A. Aviles, R. Aviles, J. Albizuri, L. Pallares-Santasmartas, and A. Rodriguez, Effect of Shot-Peening and Low-Plasticity Burnishing on the High-Cycle Fatigue Strength of DIN 34CrNiMo6 Alloy Steel, *Int. J. Fatigue*, 2019, **119**, p 338–354
 28. X. Li, J. Zhang, B. Yang, J. Zhang, M. Wu, and L. Lu, Effect of Micro-shot Peening, Conventional Shot Peening and Their Combination on Fatigue Property of EA4T Axle Steel, *J. Mater. Process. Technol.*, 2020, **275**, p p116320
 29. F. Klocke, J. Gomes, C. Löpenhaus, and R.R. Rego, Assessing the Heterogeneity of Residual Stress for Complementing the Fatigue Performance Comprehension, *J. Strain Anal. Eng. Des.*, 2016, **51**(5), p 347–357
 30. B. Fultz and J. Howe, *Diffraction Line Shapes. Transmission Electron Microscopy and Diffractometry of Materials*, 4th ed., Springer, Berlin, 2013, p 429–462
 31. J. Gubicza, N.Q. Chinh, J.L. Lábár, Z. Hegedűs, P. Szommer, G. Tichy, and T.G. Langdon, Delayed Microstructural Recovery in Silver Processed by Equal-Channel Angular Pressing, *J. Mater. Sci.*, 2008, **43**(16), p 5672–5676. <https://doi.org/10.1007/S10853-008-2817-5>
 32. B.N. Mordiyuk, Y.V. Milman, M.O. Iefimov, G.I. Prokopenko, V.V. Silberschmidt, M.I. Danylenko, and A.V. Kotko, Characterization of Ultrasonically Peened and Laser-Shock Peened Surface Layers of AISI, 321 Stainless Steel, *Surf. Coat. Technol.*, 2008, **202**, p 4875–4883
 33. V. Ji, Y.G. Zhang, and C.Q. Chen, Characterization of Ultrasonically Peened and Laser-Shock Peened Surface Layers of AISI, 321 Stainless Steel, *Surf. Coat. Technol.*, 2000, **130**(1), p 95–99
 34. N. Saklakoglu, S. Gencalp Irizalp, E. Akman, and A. Demir, Near Surface Modification of Aluminum Alloy Induced by Laser Shock Processing, *Opt. Laser Technol.*, 2014, **64**, p 235–241
 35. S. Gencalp Irizalp and N. Saklakoglu, *Laser Peening of Metallic Materials. Comprehensive Materials Finishing*, Elsevier, Amsterdam, 2016, p 408
 36. K. Li, X.S. Fu, R.D. Li, W.L. Zhou, and Z.Q. Li, A Mechanism Study on Characteristic Curve of Residual Stress FIELD in Ti–6Al–4V Induced by Wet Peening Treatment, *Mater. Des.*, 2015, **86**, p 761–764
 37. A. Zhao, J. Xie, C. Sun, Z. Lei, and Y. Hong, Effects of Strength Level and Loading Frequency on Very-High-Cycle Fatigue Behavior for a Bearing Steel, *Int. J. Fatigue*, 2012, **38**, p 46–56
 38. K. Miková, S. Bagherifard, O. Bokuvka, M. Guagliano, and L. Trško, Fatigue Behavior of X70 Microalloyed Steel After Severe Shot Peening, *Int. J. Fatigue*, 2013, **55**, p 33–42. <https://doi.org/10.1016/J.Ijfatigue.2013.04.021>
 39. S.G. Irizalp, N. Saklakoglu, E. Akman, and A. Demir, Pulsed Nd: Yag Laser Shock Processing Effects on Mechanical Properties of 6061-T6 alloy, *Opt. Laser Technol.*, 2014, **56**, p 273–277
 40. N.A. Smyth, M.B. Toparli, M.E. Fitzpatrick, and P.E. Irving, Recovery of Fatigue Life Using Laser Peening on 2024-t351 Aluminium SHEET Containing Scratch Damage: The Role of Residual Stress, *Fatigue Fract. Eng. Mater.*, 2019, <https://doi.org/10.1111/Ffe.12981>
 41. V. Singh, V. Pandey, S. Kumar, N.C.S. Srinivas, and K. Chattopadhyay, Effect of Ultrasonic Shot Peening on Surface Microstructure and Fatigue Behavior of Structural Alloys, *Trans. Indian Inst. Met.*, 2015, **69**(2), p 295–301. <https://doi.org/10.1007/S12666-015-0771-X>
 42. K. Dalaei and B. Karlsson, Influence of Overloading on Fatigue Durability and Stability of Residual Stresses in Shot Peened Normalized Steel, *Mater. Sci. Eng. A Struct.*, 2011, **528**(4), p 7323–7330. <https://doi.org/10.1016/J.Msea.2011.06.002>
 43. P.J. Withers, Residual Stress and Its Role in Failure, *Rep. Progress Phys.*, 2007, **70**(12), p 2211
 44. A. Zammit, M. Mhaede, M. Grech, S. Abela, and L. Wagner, Influence of Shot Peening on the Fatigue Life of Cu–Ni Austempered Ductile Iron, *Mater. Sci. Eng. A Struct.*, 2012, **545**, p 78–85. <https://doi.org/10.1016/J.Msea.2012.02.092>
 45. F. Takahashi, A. Tange, and K. Ando, Effect of Shot Peening on Fatigue Limit of Surface Flawed Samples, *Fatigue Fract. Eng. Mater.*, 2008, **31**(3–4), p 242–250. <https://doi.org/10.1111/J.1460-2695.2008.01219.X>
 46. J. Sakamoto, Y.S. Lee, and S.K. Cheong, Effect of Surface Flaw on Fatigue Strength of Shot-Peened Medium-Carbon Steel, *Eng. Fract. Mech.*, 2015, **133**, p 99–111. <https://doi.org/10.1016/J.Engfracmech.2014.11.005>
 47. M. Torres and H.J.C. Voorwald, An Evaluation of Shot Peening, Residual Stress and Stress Relaxation on the Fatigue Life of Aisi 4340 Steel, *Int. J. Fatigue*, 2002, **24**(8), p 877–886. [https://doi.org/10.1016/S0142-1123\(01\)00205-5](https://doi.org/10.1016/S0142-1123(01)00205-5)
 48. S.A. Meguid, G. Shagal, J.C. Stranart, K.M. Liew, and L.S. Ong, Relaxation of Peening Residual Stresses Due to Cyclic Thermo-Mechanical Overload, *J. Eng. Mater. Technol.*, 2005, **127**(2), p 170–178. <https://doi.org/10.1115/1.1867986>
 49. A. Bag, D. Delbergue, J. Ajaja, P. Bocher, M. Lévesque, and M. Brochu, Effect of Different Shot Peening Conditions on the Fatigue LIFE of 300 m Steel Submitted to High Stress Amplitudes, *Int. J. Fatigue*, 2020, **130**, p 105274. <https://doi.org/10.1016/J.Ijfatigue.2019.105274>
 50. D. Löhe and O. Vöhringer, *Stability of Residual Stresses. Handbook of Residual Stress and Deformation of Steel*, ASM, Materials Park, 2003, p 54–69
 51. K. Dalaei, B. Karlsson, and L.E. Svensson, Stability of Shot Peening Induced Residual Stresses and Their Influence on Fatigue Lifetime, *Mater. Sci. Eng. A Struct.*, 2011, **528**(3), p 1008–1015. <https://doi.org/10.1016/J.Msea.2010.09.050>

Publisher's Note Springer Nature remains neutral with regard to jurisdictional claims in published maps and institutional affiliations.